Results in Physics 6 (2016) 719–725

Contents lists available at ScienceDirect

Results in Physics

journal homepage: www.journals.elsevier.com/results-in-physics

Sintering behavior, ac conductivity and dielectric relaxation of $Li_{1.3}Ti_{1.7}Al_{0.3}(PO_4)_3$ NASICON compound

Tasiu Zangina [a,*], Jumiah Hassan [a,b], Khamirul Amin Matori [a,b], Raba'ah Syahidah Azis [a,b], Umaru Ahmadu [c], Alex See [a]

[a] Department of Physics, Faculty of Science, Universiti Putra Malaysia, 43400 UPM Serdang, Selangor, Malaysia
[b] Institute of Advanced Technology, Universiti Putra Malaysia, 43400 UPM Serdang, Selangor, Malaysia
[c] Department of Physics, Federal University of Technology, Minna, Nigeria

ARTICLE INFO

Article history:
Received 23 July 2016
Received in revised form 4 October 2016
Accepted 5 October 2016
Available online 6 October 2016

Keywords:
Sintering behavior
Dielectric permittivity
Universal power law
Electric modulus

ABSTRACT

The phenomenon of relaxation in dielectric materials is described as one of the powerful tools to determine the behavior and properties of ion transport. The kinetics of ionic species and dipole in solid-state electrolyte are dependent on frequency, temperature, and dielectric relaxation. $Li_{1+x}Ti_{2-x}Al_x(PO_4)_3$ conducting solid state electrolyte with x = 0.3 was synthesized via conventional solid state technique using the raw materials Li_2CO_3, TiO_2, Al_2O_3, and $NH_4H_2PO_4$ as starting materials. TGA/DTG and X-ray diffraction measurements were carried out to study the thermal behavior and phases of the composition. It was observed from the TGA/DTA curves that there is no mass loss above 500 °C. The XRD peaks were observed to start appearing at 500 °C which corresponds to small peaks in TGA. It was also pointed out that at increasing sintering temperatures from 700 °C to 1000 °C the number of phases drastically decreased which is attributed to the complete chemical reaction. Temperature and frequency dependence of dielectric relaxation and electric modulus of the compounds were investigated at temperatures 30–230 °C and at frequencies of 40 kHz–1 MHz. The findings showed that the dielectric relaxation peaks shift to higher temperature as frequency increases and the change in ac conductivity with frequency is in agreement with Jonscher's power law.

Introduction

Superionic conductors are material compounds that exhibit higher values of ionic conductivity within a solid state [1]. The major challenge in the study of super ionic conducting material is the electrical characterization of the material and how to reduce the conductivity temperature to ambient conditions so that they can be suitable for applications in devices such as lithium ion batteries [2–4]. NASICON is known as sodium super ionic conductor which is a family of NZP (Sodium Zirconium Phosphate). The crystal structure of the parent composition $NaZr_2(PO_4)_3$ was first determined by Hungman and Kriega [5,6]. The network structure of the NASICON $A_xM_2(XO_4)_3$ consists of a network with corner-sharing MO_6 octahedral and XO_4 tetrahedral. In such framework, each octahedron is surrounded with six tetrahedral and each tetrahedron is connected to four octahedral [7]. The NASICON-type material has an exceptional property due to its ability to provide accommodation to atoms of various sizes in its lattice sites. All the various atoms in the lattice can be substituted (Na, Zr and P) with the exception of oxygen, which may result in a material with different chemical and physical properties that may be used in diverse applications [8,9].

Most works based on NASICON have been carried out in the titanium system $LiTi_2(PO_4)_3$ (LTP) where the small size of Ti^{4+} cations make the size of the sites in the channels more appropriate for lithium cations [10]. However, it was observed that, there is also the problem of poor sinterability and controversial phase transition in the preparation of LTP [11]. But significant improvement in bulk and grain boundary conductivity was reported by Forsyth [12] due to partial substitution of Ti with Al content into the basic LTP lattice. A significant improvement has been reported by the same substitution by Aono [11]. The best optimum lithium ionic conductivity has been reported in nominal stoichiometry composition of $Li_{1+x}Ti_{2-x}Al_x(PO_4)_3$ with x = 0.3 [13]. Another important observation is that sintering of the pellets becomes more easy on substitution which reduces porosity to 4% [12]. It was also reported

* Corresponding author.
E-mail addresses: tasiuzangina@gmail.com (T. Zangina), jumiah@upm.edu.my (J. Hassan), khamirul@upm.edu.my (K.A. Matori), rabaah@upm.edu.my (R.S. Azis), u.ahmadu@yahoo.com (U. Ahmadu), alexsee1980@gmail.com (A. See).

http://dx.doi.org/10.1016/j.rinp.2016.10.003
2211-3797/

that varying sintering temperatures have an impact in increasing the number of impurity phases in the material and this has a great effect on the bulk conductivity of the material [14]. Four phases could be associated with the preparation of NASICON polycrystalline materials namely berlinite polymorphs $AlPO_4$, tridymite Al (PO_4), rutiles TiO_2 and TiP_2O_7 [15]. Based on literature reports it has been suggested that low sintering temperature (900–1000 °C) could be better for sintering LATP material to avoid loss of lithium in the sample when sintered at high temperature [16].

Dielectric relaxation study is very important and valuable phenomena for understanding the transport behavior of ions in solid state ionic conductors. Literature survey shows that dielectric properties of ionic LATP conductors have not been widely studied despite their importance which may be attributed to complexity of data representation. There is a considerable amount of research work on synthesis and electric characterization of LATP by various researchers, but only a few exist on the dielectric properties of LATP. Most of the electrical characterization on the material has been on impedance spectroscopy within the range of 1 Hz–10 MHz and just very few reported on the dielectric relaxation behavior [17].

In this research work, synthesis of LATP has been carried out using conventional solid state synthesis technique at different sintering temperatures (800–1000 °C). Structural characterization was also carried out using XRD analysis. The present study aims to report the electrical properties, dielectric permittivity, dielectric relaxation and electric modulus of sintered $Li_{1+x}Ti_{2-x}Al_x(PO_4)_3$ (LATP) compounds with x = 0.3 at the temperature range 30–230 °C and in the frequency range 40 Hz–1 MHz.

Materials and method

Materials of AR grade were used as basic starting raw materials, Li_2CO_3 (99% Alfa Aesar), TiO_2 (99.9% Alfa Aesar), $NH_4H_2PO_4$ (98% Alfa Aesar), Al_2O_3 (96% Strem) in stoichiometric amount. The stoichiometry mixture is mixed in methanol and ball-mixed for 24 h and then dried in an oven for 24 h. The virgin powder was thermally characterized using TGA measurements to identify their thermal stability. The readings were carried out from room temperature to 1000 °C at the heating rate of 10 °C/min in air using TGA/SDTA851e machine from Metler Toledo Brnd. The powder was then calcined (pre-sintered) at increasing temperatures in the range 500, 600, and 700 °C in an alumina crucible for about 2 h in air at a heating rate of 2 °C/min in order to release volatile products such as carbon dioxide, ammonia and water content from the heated mixture. The overall chemical reaction is as follows.

$$(1+x)/2Li_2CO_3 + (2-x)TiO_2 + x/2Al_2O_3 + 3NH_4H_2PO_4 = Li_{1+x}Al_xTi_{2-x}(PO_4)_3 + (1+x)/2CO_2 + 3NH_3 + 9/2H_2O$$

Suitable amount of Polyvinyl Alcohol (PVA) about 1–2% solution was added to the obtained powder as binder. The powder with PVA were mixed evenly and ground uniformly for about 1 h. The mixed powders were pressed into pellets of 12.5 mm diameter 2.5 mm thickness using uniaxial hydraulic press at a pressure of 7 tons. The sintering of the pellets was carried out at temperatures 800, 900 and 1000 °C for 2 h. The synthesis route adopted in this research is as described by Aono [11], but in this case the calcination and sintering temperatures were chosen to be lower than the longer period of ball mixing duration of about 24 h.

X-ray diffraction (XRD) measurements were performed on the calcined powders and the sintered pellets to confirm the formation of the correct crystalline structure and the phase transformations of the samples. The measurement was carried out using (Philips X'pert diffractometer model 7602 EA Almelo) Cu Kα radiation source with λ = 1.5418 Å the diffraction patterns were recorded at room temperature in 2θ scanning range from 20° to 70°. The analysis and interpretation of the XRD patterns was carried out for all the samples sintered at different sintering temperatures using the database of the Inorganic Crystal Structure Database (ICSD) by employing High Score X-part plus software version 3.0e. Crystallite size of the samples sintered can be calculated using Scherrer equation $D = \frac{k\lambda}{\beta\cos\theta}$ where D is the crystallite size, k is the shape factor and λ is the X-ray wavelength, β is the FWHM in radian and θ is Bragg angle. The X-ray density ρ_{xrd} of the samples sintered at different temperatures were calculated using the following equation $\rho_{xrd} = \frac{nM}{VN_A}$, where ρ_{xrd} is the X-ray density; n is the number of atoms per cell at each vertices which is equal to 6 atoms at each vertices for hexagonal crystal system. *M* is the molecular weight of the sample; which molecular weight of the sample is 383.28 g/mol. N_A is the Avogadro's number; and V is the unit cell volume, which is obtained from the lattice parameters. For dielectric measurements, both surfaces of the cylindrical pellets were coated with silver paste to serve as electrodes. Acquisition of data was carried out using Agilent 4294A precision impedance analyzer with an LT furnace in the frequency range 40 Hz–1 MHz at temperatures 30–230 °C. The dielectric constant of the sample was obtained using the relation $\varepsilon' = C'(t/A)$ and dielectric loss using the formula $\varepsilon'' = (G/\omega)(t/A)$ where C and G are measured capacitance and conductance respectively. The ac conductivity and electric modulus calculations were carried out using the dielectric parameters where $\sigma_{ac} = \omega\varepsilon_o\varepsilon_r''$. The Jonscher's power law is used to explain the frequency dependence of ac conductivity.

Results and discussion

TGA–DTG analysis

Thermal analysis was carried out on the LATP sample; Fig. 1 shows the curves of thermogravimetry analysis (TGA) and differential thermogravimetry (DTG). The figure illustrated the variation of mass loss with temperature. From the TGA curve we observed three regions of mass loss and one region for the sample stability. The onset mass loss occurred in region I, which is associated with the loss of water (moisture) at 172 °C. The second mass loss was observed in region II from 172 to 341 °C which is due to the decomposition of ammonium phosphate $(NH_4H_2PO_4)$ and the one in region III is associated with the decomposition of lithium carbonate (Li_2CO_3). The mass loss in region II and III is due to the loss of NH_3 and CO_2 respectively. In region IV the sample attained

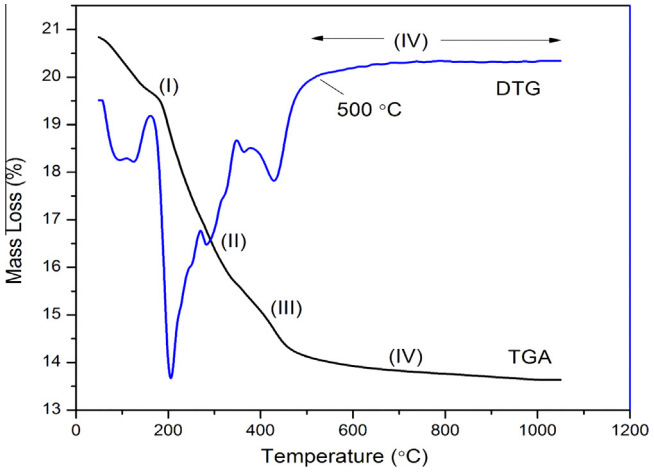

Fig. 1. TGA/DTG profile of LATP mixture powder.

stability at 500 °C beyond which there was no more mass loss as indicated on both TGA and DTG curves. The peaks of DTG curve confirmed all the decomposition processes on the TGA curve. This is similarly reported by Key [18] in which the sample was obtained via solution-based method for the first time. In the report he observed that XRD peaks appear for the first time above 500 °C which correspond to small peak in TGA. Similarly in this study we observed small XRD peaks at 500 °C as shown in Fig. 2.

X-ray diffraction analysis

Fig. 2 indicates the typical XRD patterns of the samples sintered at different sintering temperatures 500–1000 °C. The Rietveld analysis shows that all samples have a rhombohedra crystal structure with R3c space group with ICSD card no 98-006-9677. Additional peaks were observed in samples sintered at 500 °C and 600 °C which include Anatase (TiO_2) (ICSD card No. 98-005-1543), Rutile (TiO_2) (ICSD card No.98-008-1804), Titanium Phosphate (TiP_2O_7) (ICSD card No. 98-005-0110) and Aluminum phosphate ($Al(PO_4)$) (ICSD card No. 98-002-6280). These are impurity phases which occur due to lower temperature of crystallization.

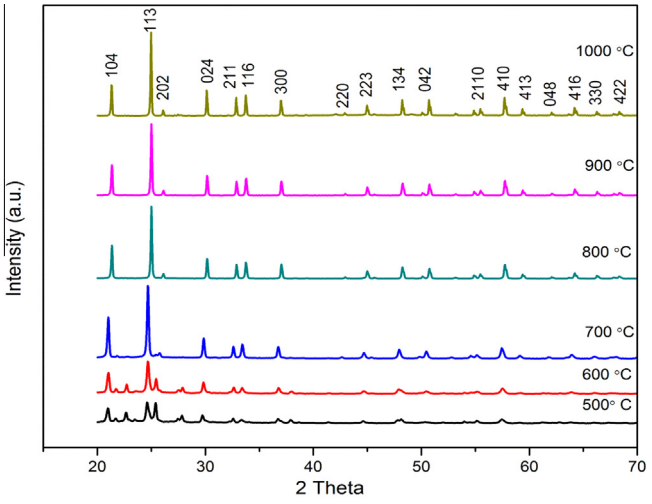

Fig. 2. XRD spectra of the LATP sintered at different sintering temperatures (500 °C, 600 °C, 700 °C, 800 °C, 900 °C, 1000 °C).

As sintering temperature increases from 700 °C to 1000 °C the number of phases decrease and disappear due to successful complete chemical reaction where only aluminum phosphate ($AlPO_4$) is present which is usually unavoidable in a high temperature heat treatment [19]. Another observation is that as the sintering temperature increases the XRD peaks corresponding to LTP phase at $2\theta = 24.67°$ with hkl 113 at 700 °C starts to shift to the right of 2θ up to 1000 °C. The results confirmed that the XRD peaks shift towards lower or high values of 2θ when doped causing changes in the lattice parameters [20]. It can be seen from Tables 1 and 2 that the unit cell parameters and volume of unit cell decrease compared with the values of LTP reported in the literature [21]. The changes (decrease) in the unit cell parameters is associated with the substitution of Ti^+ cations (0.605 Å) with smaller Al^+ size (0.535 Å) [22]. Changes in d-spacing have also been observed which contribute in peaks shifting towards high values of 2θ as tabulated in Table 2.

The relationship between sintering temperature and crystal size is given in Fig. 3. It is also observed from Table 2 that the crystallite size increases as sintering temperature increases. This is due to the increase of atomic kinetic mobility which leads to the grain growth and causes better crystallization. Experimental and theoretical densities are presented in Table 1.

Electrical conductivity analysis

ac conductivity

The parallel conductance and capacitance measurements were obtained and converted to appropriate values to calculate the ac conductivity $\sigma(\omega)$. The total conductivity $\sigma(\omega)$ is the sum of dc and ac conductivities which is related and analyzed by Jonscher's universal power law equation [23].

$$\sigma(\omega) = \sigma_{dc} + A\omega^n \quad (1)$$

where σ_{dc} is the dc conductivity, the frequency independent conductivity. The ac conductivity $\sigma_{ac}(\omega)$ obeys the Almond-West universal power law which is described as

$$\sigma_{ac}(\omega) = A\omega^n \quad (2)$$

where A is ac coefficient which is temperature dependent quantity, both A and σ_{dc} are regarded as thermally activated quantities [24] and n is the frequency exponent of the mobile ions and with the range, $0 < n < 1$. The quantity $\sigma_{ac}(\omega)$ is frequency dependent con-

Table 1
Unit cell parameters and unit cell volumes were obtained from XRD data by Reitveld refinement assuming hexagonal symmetry [19] a(Å) = 8.512 and c(Å) = 20.858 and V($Å^3$) = 1308.78.

Sintering temp. (°C)	Molecular mass (g/mol)	Unit cell parameters			Experimental density (g/cm^3)	Theoretical density (g/cm^3)
		a(Å)	c(Å)	V($Å^3$)		
800	383.28	8.5089	20.8477	1307.181	2.40	2.80
900	383.28	8.5081	20.8357	1306.183	2.44	2.92
1000	383.28	8.5110	20.8430	1307.532	2.81	2.92

Table 2
Crystal size calculated using the Scherrer calculator after Reitveld refinement analysis.

Sintering temp. (°C)	2Theta (deg)	FWHM (β) (deg)	d-spacing	Crystal Size (μm)
500	24.6207	0.2970	3.6129	2.74
600	24.6705	0.2531	3.6057	3.22
700	24.6655	0.1894	3.6065	4.30
800	24.9941	0.1258	3.5598	6.47
900	24.9953	0.1188	3.5596	6.86
1000	25.0491	0.1000	3.5521	8.14

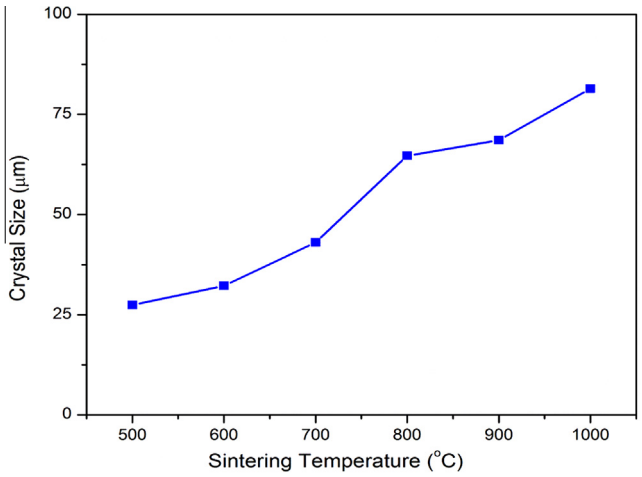

Fig. 3. Variation of crystal size with sintering temperatures.

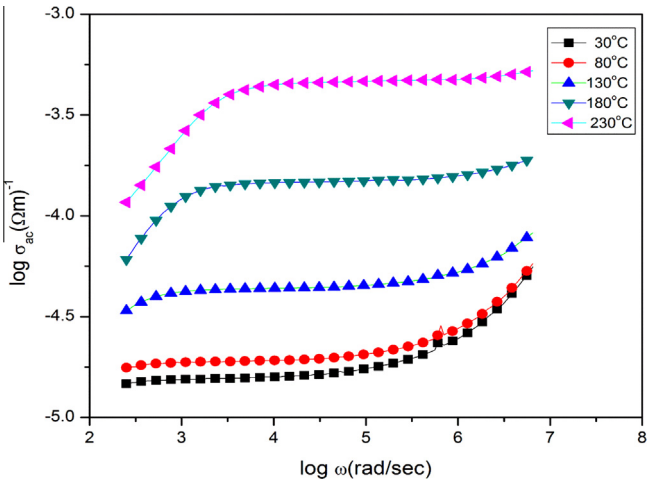

Fig. 5. Plot of log σ_{ac} vs logω at various temperatures.

ductivity which is used to analyze and understand the dynamics of ions in NASICON-type materials [25]

The variation of ac conductivity $\sigma_{ac}(\omega)$ with frequency f, in log-log scale at different temperatures is shown in Fig. 4. The experimental σ_{ac} conductivity well fit Jonscher's power law. In all the plots two regions are visible and it is observed that at low temperature from room temperature 30–130 °C, the conductivity increases gradually. They are frequency-independent in the low frequency regions (from 40 Hz to 10 kHz in the plateau region) and this is considered as dc conductivity at low frequencies which is related with the transport of Li^+ ions [26]. The conductivity then increases rapidly at high frequency region from 10 kHz to 1 MHz which is considered to be frequency dependent and is less temperature dependent from the power law $\sigma(\omega)\alpha\omega^n$. Similar behavior was obtained by Govindaraj [24] on the ac conductivity analysis of $Na_5Ti(PO_3)_4$. At high temperatures (180 °C and 230 °C) the data analysis of the conductivity shows rapid increase in conductivity at low frequency region (40 Hz–1 kHz) and gradually increases and disperses at high frequency region (1 kHz–1 MHz). Fig. 4 exhibits a typical ionic conductivity behavior of ionic materials. At high frequency region the conductivity exhibits frequency dependence and dc plateau at low frequency region. The increasing tendency of ac conductivity as frequency increases may be predicted to be due to the disorder of cations in their sites and also due to the presence of space charge. The value of ac conductivity obtained at 30 °C is $5.58 \times 10^{-5}\,(m\Omega)^{-1}$. The highest ac conductivity obtained at 230 °C is $5.24 \times 10^{-4}\,(m\Omega)^{-1}$. Low temperature ac conduction is associated with the bipolar hopping mechanism, whereas, high temperature conduction is attributed to thermally activated polaron hopping [27]. The lower value of ac conductivity is ascribed to the presence of $AlPO_4$ impurity in the compound which significantly decreases the conductivity of the material [28].

The values of correlation exponent n has been determined from the slopes of log $\sigma_{ac}(\omega)$ vs log ω as shown in Fig. 5. Eq. (2) was used to calculate the values of n at different temperatures. It is observed from the results of Fig. 6 that n decreases with an increase in temperatures, the values obtained vary from 0.30 at 30 °C (at room temperature) to 0.02 at high temperature of 230 °C. Moreover, the result indicates that the mobility of the ions at high temperature is frequency independent conductivity and also n is temperature-dependent and obeys power law since the values of n are within the range $0 < n < 1$. Similarly the values obtained by some authors are also within the range where the study of $Na_{1+x}Ti_{2-x}Al_x(PO_4)_3$ [29] reported $n \sim 0.6$ for the compositions. The study of $Na_5Ti(PO_4)_3$ glass [30] reported similar values within the range.

Fig. 7 shows the plots of $\ln\sigma_{ac}$ as a function of reciprocal temperature (1000/T) of the sample (LATP) at selected frequencies sintered at 1000 °C. It can be seen that the temperature dependence of

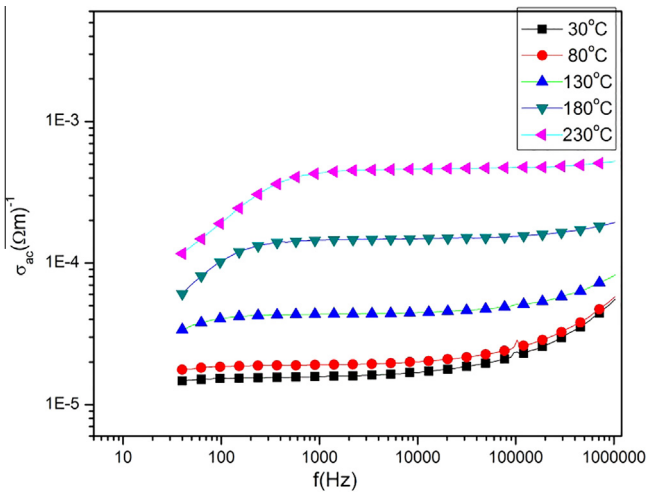

Fig. 4. Variation of ac conductivity with a function of frequency at various temperatures.

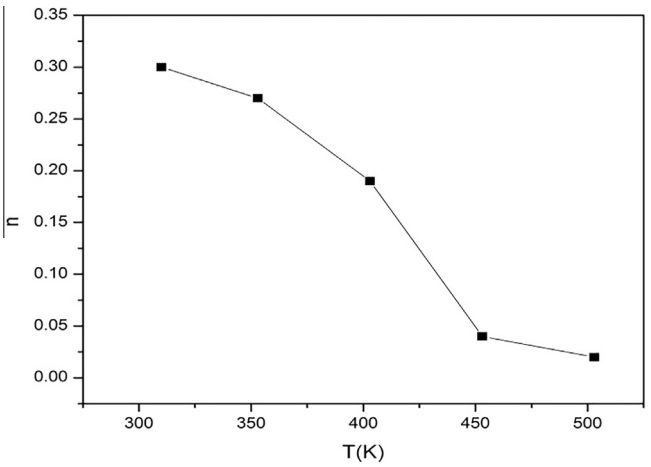

Fig. 6. Plot of correlation exponent n vs temperature (K) of LATP.

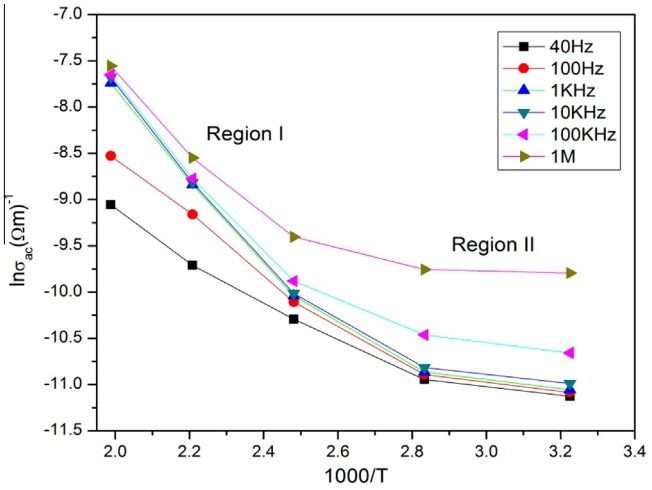

Fig. 7. Variation of $\sigma_{ac}(w)$ as a function of 1000/T at different frequencies of LATP.

the ac conductivity has two regions, region I and region II. This is attributed to different conduction mechanisms. The conductivity increases as temperature increases. The LATP solid ionic conductor has carrier ions Li^+ that are thermally excited due to temperature increase. Temperature increase causes more charge ions carriers to overcome the minimum energy and electrical conductivity is observed in the system. Two conduction mechanisms have been observed one at low temperature and another at high temperature. The temperature dependent conductivity is represented by the following relation (Arrhenius equation):

$$\sigma = \sigma_o \exp(-\Delta E/kT) \quad (3)$$

where σ_o is the pre-exponential factor, ΔE is the activation energy for the ion Li^+ transfer, k is the Boltzmann constant and T is the temperature in kelvin. Activation energies E_I and E_{II} can be calculated using Eq. (3) from the slopes of linear portions of Fig. 7 at different frequencies in region I and region II. At low frequency of 40 Hz the activation energies E_I and E_{II} in region I and region II are 0.21 eV and 0.04 eV respectively. However, at high frequency of 1 MHz the activation energies in region I and region II are 0.32 eV and 0.008 eV respectively. Figs. 4, 5 and 7 clearly indicate that in the low frequency part, the ac conductivity is more sensitive to temperature, whereas the conductivity is temperature-independent at high frequency.

Dielectric permittivity analysis

Dielectric constant and dielectric loss

Fig. 8(a) and (b) show the dielectric properties of the material ε′ and ε″ (real and imaginary parts of complex permittivity respectively) in the frequency range 40 Hz–1 MHz at different temperatures from 30 °C to 230 °C. Similar trends have been observed for all the curves at different temperatures for both ε′ and ε″.

Fig. 8(a) illustrates that the dielectric constant ε′ decreases with increasing frequency. The decrease in the dielectric constant with increasing frequency is observed to be rapid at lower frequency and gradually at high frequency. This may be attributed to normal behavior of dielectric materials and also due to the relaxation behavior of the system [27]. The material response to dielectric constant is mainly due to the contribution of polarization mechanisms which may be electronic, ionic, dipole and space charge polarizations. Frequency increase causes dipoles not having enough rapid rotation. Due to this the oscillation lags behind and the dielectric constant decreases gradually. At high frequency dipoles ceases to follow the field and polarization is stopped and the dielectric constant decreases to approach a constant value in the frequency range 1 kHz–1 MHz. From the figure it can be seen that the sample shows high value of dielectric constant at a frequency lower than 1 kHz. This is because at low frequencies the ions do have enough time to accumulate at the interface of the conducting regions which cause the dielectric constant to increase, but at high frequencies the ions do not have sufficient time to accumulate at the interface and there will be no polarization [31]. At high temperatures and within the low frequencies regions of all the plots the dielectric constant is due to the movement of ions (charge carriers) which increases with rise in temperature. The effect of temperature in this case is regarded as interfacial polarization not dipolar polarization. At high temperature and within the high frequency region, loss of dispersion increases which is attributed to thermal vibration and no time for the material to respond to the applied electric field. This suggests that at high frequency the interfacial polarization is insignificant hence the dielectric constant maintains constant value within the frequency range 10 kHz–1 MHz.

Fig. 8(b) shows the effect of frequency on the dielectric loss (imaginary part of complex permittivity) at various temperatures

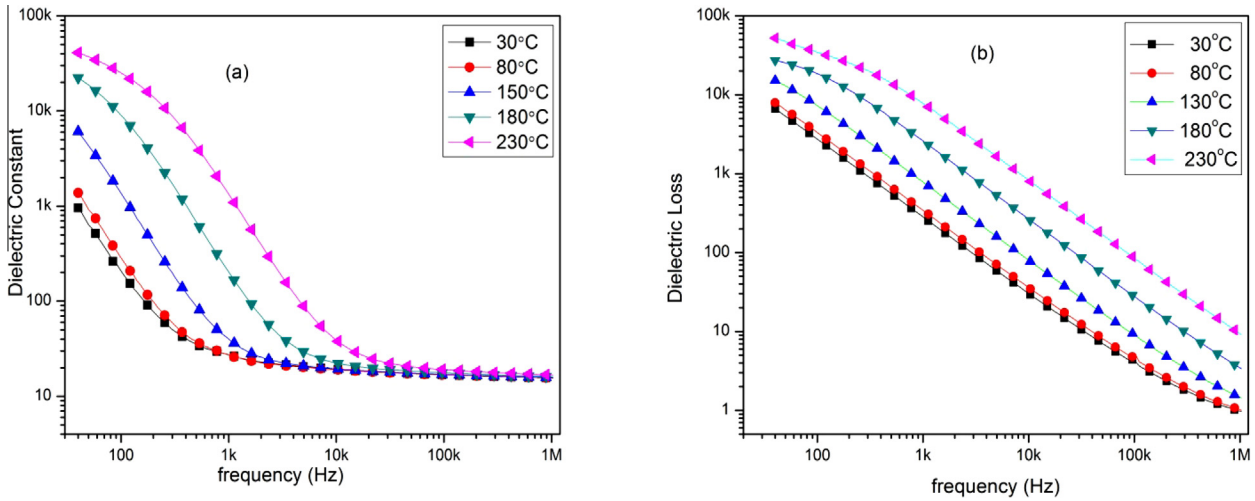

Fig. 8. Frequency dependence of (a) Plot of real part of dielectric permittivity (dielectric constant) against frequency at different temperatures for LATP. (b) Plot of imaginary part of dielectric permittivity (dielectric loss) against frequency at different temperatures.

from 30 °C to 230 °C. Dielectric loss is the power loss or the amount of electric power dissipated within a material under the influence of the applied field. From the observed variation of ε″ with frequency and temperature it can be seen that the dielectric loss decreases with increasing frequency and increases with the raise in temperature from 30 to 230 °C. This effect of frequency and temperature on the dielectric loss of the material is ascribed to the formation of interfacial polarization within the sample interface and at the electrodes [25]. The analysis of the results also exhibits that the dielectric loss ε″ follows the power law with frequency ω [32] as shown in Eq. (4).

$$\varepsilon'' = B\omega^{m} \tag{4}$$

where m is the frequency power factor and B is a constant. A plot of lnε″ versus lnω shows straight lines at the various temperatures. The values of m were obtained from the slopes of the graph at different temperatures using Eq. (4). It has been observed that the values of m tend to decrease as temperature increases.

Fig. 9 shows the plots of real part of dielectric permittivity with temperature indicating the temperature dependence of dielectric constant at different frequencies for the LATP sample. As temperature increases the dielectric constant also increases. The increment in the dielectric constant ε′ due to rise in temperature is observed to be high in the frequency range 40 Hz–10 kHz. This is ascribed by the interfacial polarization and presence of space charge. At higher frequencies 100 kHz–1 MHz there is very low or even negligible increase in dielectric constant with raise in temperature, hence at these frequencies, the dielectric constant ε′ is temperature-independent. This is because at high frequency there is no accumulation of charges at the interface therefore, there will be no interfacial polarization and the space charge effect is absent.

Electric modulus analysis

Electrical modulus representation is widely used to analyze the conductivity behavior of ionic conductors. The electric modulus theory is an important technique to predict the relaxation behavior of ionic conductors and polymer composites. It gives an opportunity to explore the conductivity and associated relaxations in materials. In a physical manner, electric modulus is comparatively analogous to relaxation of electric field in materials when the electric displacement maintains a constant value [32,33]. The complex dielectric modulus M*(ω) is defined as the inverse of complex dielectric constant and evaluated as follows [32,34].

$$M^{*} = M' + iM'' = \frac{1}{\varepsilon^{*}(\omega)} = \frac{1}{\varepsilon'(\omega) + i\varepsilon''(\omega)} \tag{5}$$

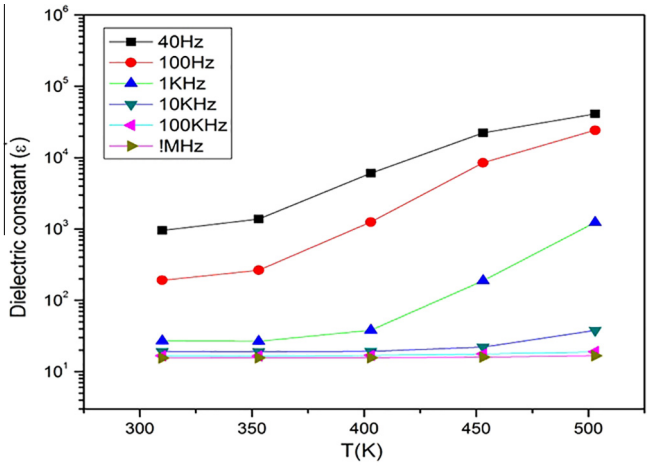

Fig. 9. Temperature dependence of e' at different frequencies.

where M′ and M″ are calculated from the values of ε′ and ε″ and $M' = \frac{\varepsilon'}{\varepsilon'^2+\varepsilon''^2}$, $M'' = \frac{\varepsilon''}{\varepsilon'^2+\varepsilon''^2}$

M′ and M″ are the real and imaginary part of dielectric modulus respectively. Frequency dependence of real and imaginary part of the dielectric modulus of the sample at different temperatures is shown in Figs. 10 and 11.

The plot of Fig. 10 shows that the values of M' tend to approach zero at low frequencies from 40 Hz to 10 kHz for all the temperatures. This is attributed to non-contribution of electrode effects in the system i.e. the electrode polarization effect is negligible towards M′. M′ increases gradually as the frequency increases and above 100 kHz, it tends to approach constant values. These phenomena of M′ at high frequency may be associated with the absence of space charge effect. It is also noticed that the M′ decreases with increase in temperature within the frequency range as shown in Fig. 10.

Fig. 11 shows the plot of the imaginary part of dielectric modulus with frequency at different temperatures. It can be seen from the graphs that M″ rise gradually to a maximum (maximum peak) and then decreases subsequently at high frequency for all the temperatures. It is also observed that the positions of the peak of M″ shifts from lower frequency towards higher frequency region and the height of the peak increases gradually as the temperature rises from 30 °C to 230 °C. This confirms the presence of dielectric

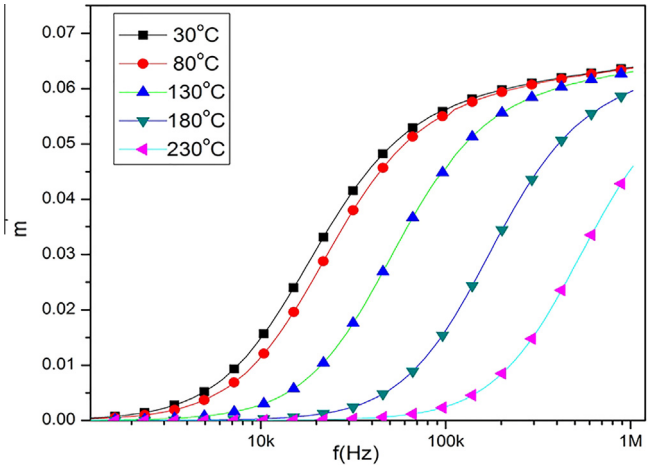

Fig. 10. Frequency dependence of dielectric modulus m′ (Real part) at various temperatures.

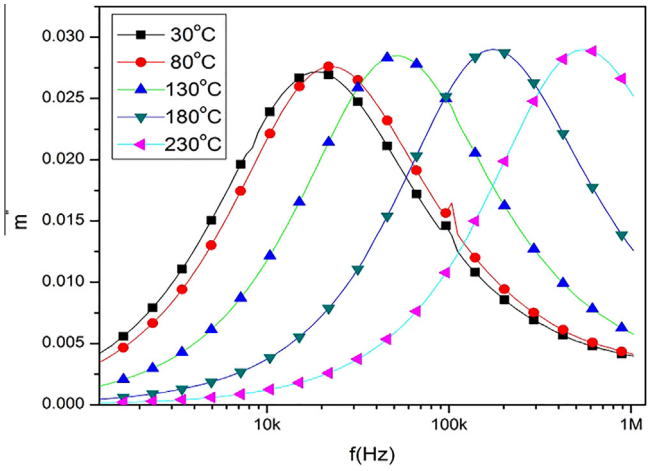

Fig. 11. Frequency dependence of dielectric modulus m″ (imaginary part) at various temperatures.

relaxation that is thermally activated and the predominant hopping process of the ions (charge carriers). It is indicated that in the low frequency region. The ions move to a long range mobility, whereas in the high frequency region, the ions (charge carriers) are confined to potential wells and only able to move freely on a short distance within the wells [35].

Conclusion

LATP samples were synthesized by means of conventional solid state reaction technique. Sintering properties of the material were studied at various temperatures from 500 to 1000 °C. X-ray Diffraction studies confirmed the rhombohedra structure with R3c space group of the synthesized sample with ICSD card No. 98-006-9677. AC conductivity behavior of the material was investigated; and the material shows typical ionic conductivity behavior of an ionic material. In the high frequency region the conductivity exhibits frequency-dependence. The decrease in the value of correlation exponent with the increase in temperature confirms that the mobility of the ions at high temperature is frequency independent conductivity and also n is temperature-dependent which obeys the power law. The decreasing trend for both dielectric constant and dielectric loss with increasing frequency were observed at all temperatures. The presence of dielectric relaxation was confirmed by investigating the variation of electric modulus with frequency in which the peak values of M″ shift from lower frequency towards the high frequency region and the height of the peak increases gradually as the temperature rises.

Acknowledgements

This research work was financially supported by the Fundamental Research Grand Scheme (FRGS) Project No.: 01-02-14-1599FR. The authors gratefully acknowledge Department of Physics, Faculty of Science, Universiti Putra Malaysia for the facilities provided.

References

[1] Hull S, Facility TI. Superionics: crystal structures and conduction processes. Rep Prog Phys 2004;67:1233–314.
[2] Choi N, Chen Z, Freunberger SA, Ji X, Sun K, Amine K, Yushin G, Nazar LF, Cho J, Bruce PG. Challenges facing lithium batteries and electrical double-layer capacitors. Angew Chem Int Ed 2012;51:9994–10024. doi: http://dx.doi.org/10.1002/anie.201201429.
[3] Pistoia G. Lithium-ion batteries advances and applications. first ed. Poland: Elsevier; 2014.
[4] P.M. GroupM. Division. Solid electrolytes general principles, characterization materials, applications. New York: Academic Press; 1978.
[5] Alamo J. Crystal chemistry of the NaZra(PO_4)$_3$, NZP or CTP, structure family. J Mater Sci 1986;21:444–50.
[6] Ove Hagman Lors, Kierkegaard Peder. The crystal structure of NaMe(PO_4)$_3$. Acta Chem Scand 1968;22:1822–32.
[7] Wang GX, Bradhurst DH, Dou SX, Liu HK. LiTi2(PO_4)$_3$ with NASICON-type structure as lithium-storage materials. J Power Sources 2003;124(1):231–6.
[8] Ahmadu U, Musa AO, Jonah SA, Rabiu N. Synthesis and thermal characterization of NZP compounds $Na_{1-x}Li_xZr_2(PO_4)_3$ (x = 0.00 – 0.75). J Therm Anal Calorim 2010;101:175–9. doi: http://dx.doi.org/10.1007/s10973-010-0679-y.
[9] Petkov VI, Egorkova OV. On the existence of phases with a structure of $NaZr_2(PO_4)_3$ in series of binary orthophosphates with different alkaline element to zirconium ratios. J Struct Chem 1996;37:933–40.
[10] Maldonado-Manso Pilar, Losilla Enrique R, Martínez-Lara María, Aranda Miguel AG, Bruque Sebastián, Mouahid Fatima E, Zahir Mohammed. High lithium ionic conductivity in the $Li_{1+x}Al_xGe_yTi_{2-x-y}(PO_4)_3$ NASICON series. Chem Mater 2003;15:1879–85.
[11] Aono H, Sugimoto E, Sadaoka Y, Imanaka N, Adachi G. Electrical property and sinterability of $LiTi_2(PO_4)_3$ mixed with lithium salt (Li_3PO_4 or Li_3BO_3). Solid State Ionics 1991;47:257–64.
[12] Forsyth M. NMR studies of modified NASICON-like, lithium conducting solid electrolytes. Solid State Ionics 1999;124:213–9.
[13] Wong Shan, Newman Peter J, Best AS, Nairn KM, MacFarlane DR, Forsyth M. Towards elucidating microscopic structural changes in Li-ion conductors $Li_{1+y}Ti_{2-y}Aly[PO_4]_3$ and $Li_{1+y}Ti_{2-y}Al_y[PO4\ ]_{3-x}\ [MO_4]_x$(M = V and Nb): X-ray and ^{27}Al and ^{31}P NMR studies. J Mater Chem 1998;8:2199–203.
[14] Best AS, Newman PJ, MacFarlane DR, Nairn KM, Wong S, Forsyth M. Characterization and impedance spectroscopy of substituted $Li_{1.3}Al_{0.3}Ti_{1.7}(PO_4)_{3-x}\ (ZO_4)_x$ (Z= V, Nb) ceramics. Solid State Ionics 1999;126:191–6.
[15] Best AS, Forsyth M, MacFarlane DR. Stoichiometric changes in lithium conducting materials based on $Li_{1+x}Al_xTi_{2-x}(PO_4)_3$: Impedance, X-ray and NMR studies. Solid State Ionics 2000;136–137:339–44.
[16] Huang L, Wen Z, Wu M, Wu X, Liu Y, Wang X. Electrochemical properties of $Li_{1.4}Al_{0.4}Ti_{1.6}(PO_4)_3$ synthesized by a co-precipitation method. J Power Sources 2011;196:6943–6.
[17] Ramaraghavulu R, Buddhudu S. Analysis of structural, thermal and dielectric properties of $LiTi_2(PO4)_3$ ceramic powders. Ceram Int 2011;37:3651–6.
[18] Key B, Schroeder DJ, Ingram BJ, Vaughey JT. Solution-based synthesis and characterization of lithium-ion conducting phosphate ceramics for lithium metal batteries. Chem Mater 2012;24:287–93.
[19] Fu J. Superionic conductivity of glass-ceramics in the system Li_2O–Al_2O_3–TiO–P_2O_5. Solid State Ionics 1997;96:195–200.
[20] Kothari DH, Kanchan DK. Study of Study of electrical properties of gallium-doped lithium titanium aluminum phosphate compounds. Ionics 2015;21:1253–9. doi: http://dx.doi.org/10.1007/s11581-014-1287-9.
[21] Aono H. Ionic conductivity and sinterability of lithium titanium phosphate system. Solid State Ionics 1990;40–41:38–42.
[22] Arbi K, Bucheli W, Jiménez R, Sanz J. High lithium ion conducting solid electrolytes based on NASICON $Li_{1+x}\ Al_x\ M_{2-x}(PO_4)_3$ materials (M = Ti, Ge and $0 \leqslant x \leqslant 0.5$). J Eur Ceram Soc 2015;35:1477–84.
[23] Jonscher AK. Dielectric relaxation in solids. London: Chelsea Dielectric; 1983.
[24] Govindaraj G, Mariappan CR. Synthesis, characterization and ion dynamic studies of NASICON type glasses. Solid State Ionics 2002;147:49–59.
[25] Mariappan CR, Go G. Ac conductivity, dielectric studies and conductivity scaling of NASICON materials. Mater Sci Eng B 2002;94:82–8.
[26] Mariappan CR, Govindaraj GT. Conductivity and ion dynamic studies in the $Na_{4.7+x}Ti_{1.3-x}(PO4)_{3.3}-x$ ($0 \leqslant x \leqslant 0.6$) NASICON material. Solid State Ionics 2005;176:1311–8.
[27] Prakash Nautiyal Om, Bhatt SC, Pant RP, Semwal BS. Dielectric properties of silver sodium niobate mixed ceramic system. Indian J Pure Appl Phys 2010;48:357–62.
[28] Xiaoxiong Xu ZL, Wen Zhaoyin, Gu Zhonghua, Xu Xiaohe. Lithium ion conductive glass ceramics in the system $Li_{1.4}Al_{0.4}(Ge_{1-x}Ti_x)_{1.6}(PO_4)_3$ (x = 0–1.0). Solid State Ionics 2004;171:207–13.
[29] Mouahid FE, Zahir M, Maldonado-manso P, Bruque S, Losilla ER, Chimie D, Doukkali C, Jadida E. Na–Li exchange of $Na_{1+x}Ti_{2-x}Al_x(PO_4)_3$ ($0.6 \leqslant x \leqslant 0.9$) NASICON series: a Rietveld and impedance study. J Mater Chem 2001;3:3258–63.
[30] Mariappan CR, Govindaraj G, Rathan SV, Prakash GV. Preparation, characterization, ac conductivity and permittivity studies on vitreous $M_4AlCdP_3O_{12}$ (M = Li, Na, K) system. Mater Sci Eng B 2005;121:2–8.
[31] Maxwell J. A treatise on electricity and magnetism, 1973. p. 828.
[32] Attia AA, Soliman HS, Saadeldin MM, Sawaby K. AC electrical conductivity and dielectric studies of bulk p-quaterphenyl. Synth Met 2015;205:139–44.
[33] Liu Jianjun. Dielectric permittivity and electric modulus in $Bi_2Ti_4O_{11}$. J Chem Phys 2003;119:5.
[34] Wong YJ, Hassan J, Hashim M. Dielectric properties, impedance analysis and modulus behavior of $CaTiO_3$ ceramic prepared by solid state reaction. J Alloys Compd 2013;571:138–44.
[35] Ahmadu U, Salkus T, Musa AO, Isah KU. Electrical and dielectric characterization of $Na_{0.5}Li_{0.5}Zr_2(PO_4)_3$. Open J Phys Chem 2011:94–103. doi: http://dx.doi.org/10.4236/ojpc.2011.13013.